Title

First report of electrospun cellulose acetate nanofibers mats with chitin and chitosan nanowhiskers: Fabrication, characterization, and antibacterial activity

Authors

Pereira, Antonio GB
Fajardo, André R
Gerola, Adriana P
et al.

Publication Date

2020-12-01

DOI

10.1016/j.carbpol.2020.116954

Peer reviewed

Carbohydrate Polymers 250 (2020) 116954

Contents lists available at ScienceDirect

Carbohydrate Polymers

journal homepage: www.elsevier.com/locate/carbpol

First report of electrospun cellulose acetate nanofibers mats with chitin and chitosan nanowhiskers: Fabrication, characterization, and antibacterial activity

Antonio G.B. Pereira [a,e,f,*], André R. Fajardo [b], Adriana P. Gerola [c], Jean H.S. Rodrigues [d], Celso V. Nakamura [d], Edvani C. Muniz [e], You-Lo Hsieh [f]

[a] Universidade Tecnológica Federal do Paraná (UTFPR), Campus Dois Vizinhos (DV), Engenharia de Bioprocessos e Biotecnologia, Dois Vizinhos, PR, Brazil
[b] Universidade Federal de Pelotas, Campus Capão do Leão, Laboratório de Tecnologia e Desenvolvimento de Compósitos e Materiais Poliméricos (LaCoPol), Pelotas, RS, Brazil
[c] Universidade Federal de Santa Catarina, Departamento de Química, Florianópolis, SC, Brazil
[d] Universidade Estadual de Maringá, Departamento de Análises Clínicas, Maringá, PR, Brazil
[e] Universidade Estadual de Maringá, Grupo de Materiais Poliméricos e Compósitos (GMPC), Departamento de Química, Av. Colombo 5790, 87020-900, Maringá, PR, Brazil
[f] University of California, Davis, Biological and Agricultural Engineering, One Shields Avenue, Davis, CA, 95616, USA

ARTICLE INFO

Keywords:
Chitosan nanowhiskers
Chitin nanowhiskers
Electrospun nanofibers mats
Cellulose acetate
Physical adsorption

Chemical compounds studied in this article:
Cellulose acetate (PubChem CID: 139600838)
Chitin (PubChem CID: 6857375)
Chitosan (PubChem CID: 71853)
3-(4,5-Dimethylthiazol-2-yl)-2,5-diphenyltetrazolium bromide (PubChem CID: 64965)
Sodium hydroxide (PubChem CID: 14798)
Hydrochloric acid (PubChem CID: 313)

ABSTRACT

Physical adsorption has shown to be facile and highly effective to deposit chitosan nanowhiskers (CsNWs, 60 % deacetylated, length: 247 nm, thickness: 4–12 nm, width:15 nm) on electrospun cellulose acetate nanofibers (CANFs, 560 nm) to effect complete surface charge reversal from negatively charged CANFs (−40 mV) to positively charged CsNWs-adsorbed CANFs (+8 mV). The CsNWs coverage did not alter the smooth and homogeneous morphology of fibers, as observed from SEM images. Biological assays showed the CsNWs covered nanofibers were effective against the Gram-negative bacterium *E. coli*, reducing 99 % of colony forming units (CFU) in 24 h and atoxic to healthy Vero cells. The use of CsNWs to modify cellulose fiber surfaces has been proved to be efficient and may be applied to a broad scope of fields, especially as biomaterials and biomedical applications.

1. Introduction

Electrospinning has been recognized as a versatile technique in the preparation of ultra-fine fibrous mats (Doshi & Reneker, 1995; Xue, Wu, Dai, & Xia, 2019). Due to the ease to generate nanometer to submicron wide fibers from a great variety of polymers as well as the intrinsically high specific surface and widely possible porosity, electrospun fibers have been investigated for many applications including tissue engineering (Orlova, Magome, Liu, Chen, & Agladze, 2011; Zhang, Venugopal et al., 2008), filtration (Beier, Guerra, Garde, & Jonsson, 2006), metal ion removal (Haider & Park, 2009), drug release (Ma et al., 2011) and catalysis (Yousef et al., 2012). Among naturally derived polymers, one of particular interest is the cellulose acetate (CA), a soluble esterified-derivative of the biopolymer cellulose that can be easily electrospun into nanofibers mats (Liu & Hsieh, 2002). Not only the versatile solvent systems allow CA to be mixed with a large number of polymers and compounds (Du & Hsieh, 2009; Zhang, Hsieh, Zhang, & Hsieh, 2008), but easy hydrolysis of CA to cellulose also enables further chemical reactions to functional materials (Chen & Hsieh, 2005; Wang & Hsieh, 2004).

* Corresponding author at: Universidade Tecnológica Federal do Paraná (UTFPR), Campus Dois Vizinhos (DV), Engenharia de Bioprocessos e Biotecnologia, Dois Vizinhos, PR, Brazil.
E-mail address: guilebasso@hotmail.com (A.G.B. Pereira).

https://doi.org/10.1016/j.carbpol.2020.116954
Received 12 April 2020; Received in revised form 6 August 2020; Accepted 13 August 2020
Available online 19 August 2020

Different approaches such as addition of fillers, preparation of bicomponent fibers, surface modification, among others, have been used to provide or further improve some properties of electrospun nanofibers. Multiwalled carbon nanotubes were incorporated into cellulose nanofibers rendering fibers with improved water wettability, higher specific surface, and mechanical properties (Lu & Hsieh, 2010). The addition of ZnO nanoparticles into electrospun CA nanofibers showed improvement in both hydrophobicity and antibacterial activity (Anitha, Brabu, Thiruvadigal, Gopalakrishnan, & Natarajan, 2012). Phase-separated core--shell bicomponent nanofibers were produced by the electrospinning of CA and polyethylene oxide (Zhang & Hsieh, 2008). Cellulose fibrous membrane, obtained from hydrolysis of electrospun CA, was successfully functionalized with Cibracon Blue F3GA for lipase enzyme immobilization to enhance high catalytic rate and persistent activity compared to that from free form of lipase (Lu & Hsieh, 2009).

Surface modification takes the advantage of the high specific surface of electrospun fibers and is attractive. The negatively charged nature of CA has been utilized to deposit positive species by physical adsorption (Elashnikov, Rimpelová, Děkanovský, Švorčík, & Lyutakov, 2019), such as alternating assembling of positively charged polyethyleneimine and negatively charged graphene oxide as an ammonium sensor (Jia, Yu, Zhang, Dong, & Li, 2016) and hydroxyapatite and chitosan as corrosion resistant and bioactive coating agents in metallic implants (Zhong, Qin, & Ma, 2015). Chitin nanocrystals were used as surface modifying agents to reverse the hydrophobic nature of CA mats to render super hydrophilic electrospun mats to be used as water filtration system (Goetz, Jalvo, Rosal, & Mathew, 2016). Moreover, the biofouling and biofilm formation were significantly reduced in the coated membranes while the material presented a web-like structure with reduced pore size.

The use of bioactive chitosan is attractive due to its many attractive physicochemical and biological properties well-documented in the literature (Berger, Reist, Mayer, Felt, & Gurny, 2004). Chitosan is a linear polysaccharide composed of randomly distributed β-(1→4)-linked D-glucosamine and *N*-acetyl- *d*-glucosamine units derived from the biopolymer chitin (Berger et al., 2004), to exhibit polycationic behavior in pH conditions lower than the pKa of its amino groups (~6.5) (Dash, Chiellini, Ottenbrite, & Chiellini, 2011). This feature endows chitosan with a self-assembling ability triggered by the formation of polyelectrolyte complexes with polyanions (Quiñones, Peniche, & Peniche, 2018). Due to this ability, chitosan has been extensively studied in the modification of negatively charged surfaces due to electrostatic interaction (Antunes et al., 2011; Tu et al., 2019). Multiple alternating bilayers based on chitosan and sodium alginate (SA) can be easily assembled on CA fibers (Ding, Du, & Hsieh, 2011). Increasing such bilayers has shown to reduce the permeability of pure water and NaCl solution (Ritcharoen, Supaphol, & Pavasant, 2008).

Although the preparation of both chitin and chitosan nanocrystals, highly crystalline spindle-like material with nanometric dimensions, is well established (Bai et al., 2020; Pereira, Muniz, & Hsieh, 2014; Pereira, Muniz, & Hsieh, 2015), the use of chitosan nanowhiskers (CsNWs) to modify the surface of CA nanofibers mats have not been reported yet. Therefore, this study develops processes to fabricate electrospun CA nanofibrous mats with CtNWs incorporated in the spin dope or CsNWs adsorbed on the fiber surfaces. The focus includes how this embodiment of CsNWs in electrospun CA fibers and the effect on their surface charge properties. We hypothesize that the CsNWs coating may enhance the biological activity of the CA nanofibers, which potentiate their further use in biomedical applications.

2. Materials and methods

2.1. Materials

Cellulose acetate (CA, 39.8 % acetyl content, and M_n ≈30,000 Da); chitin from crab shells (practical grade), tryptic soy broth (TSB) and tryptic soy agar (TSA) were purchased from Sigma-Aldrich (USA). *N,N*-dimethylacetamide (DMAc, 99.8 %), acetone (P.A.), sodium hydroxide (NaOH, 97 %), potassium hydroxide (KOH, 85 %), sodium chlorite ($NaClO_2$, 80 %), hydrochloric acid (HCl, 36.5 %) were purchased from EMD Chemicals (USA). Phosphate buffer solution pH 4.0 was purchased from Dinâmica (Brazil). Dulbecco's Modified Eagle Medium (DMEM) and fetal bovine serum (FBS) were purchased from Gibco (USA). 3-(4,5-dimethylthiazol-2-yl)-2,5-diphenyltetrazolium bromide (MTT) was purchased from Gen-View Scientific Inc. (USA). All chemicals were used as received, without further purification.

2.2. Isolation of chitin nanowhiskers

Chitin nanowhiskers (CtNWs) were prepared using the same protocol described by Pereira et al. (Pereira et al., 2014, 2015) without modifications. Commercial chitin was firstly purified by removing residual proteins followed by bleaching. Proteins were removed by heating 5 g of chitin in 150 mL of KOH solution (5 w/v-%) at boil under vigorous stirring for 6 h. The suspension was kept under stirring at 25 °C for another 12 h, filtered and washed with water. Next, the collected solid was bleached in 150 mL of 1.7 % $NaClO_2$ in pH 4 buffer acetate at 80 °C for 2 h, then filtered and washed with water. The bleaching reaction was performed twice. Finally, the bleached solid was re-suspended in 150 mL of KOH solution (5 w/v-%) for 48 h, then centrifuged, washed, and oven dried (50 °C) to yield 71 % (~3.6 g).

CtNWs were obtained by hydrolyzing the purified chitin in 3 mol/L HCl at boil for 90 min under stirring. The ratio chitin/volume of HCl solution (g/mL) was fixed at 1:30. The reaction was stopped by adding 50 mL of cold water and centrifuged (3400 rpm for 15 min). The precipitate was re-suspended in 200 mL of distilled water followed by centrifugation. This procedure was repeated three times. Next, the precipitate was re-suspended in distilled water (200 mL) and dialyzed (molecular weight cut-off 12,000 g/mol) against water at room temperature (~25 °C) up to neutral pH. The suspension was sonicated (40 % maximum amplitude) for a total of 20 min with 5 min of interval between every 5 min of sonication cycle, followed by centrifugation (3000 rpm, 10 min) for removing any remaining precipitate. Finally, the CtNWs suspension was stored at 8 °C. The yield was 65 % (~2.3 g)

2.3. Synthesis of chitosan nanowhiskers

Chitosan nanowhiskers (CsNWs) were synthesized via deacetylation of the as-prepared CtNWs. For this, 50 mL of an aqueous suspension containing ~ 500 mg of CtNWs were diluted with a NaOH solution (100 mL, 50 w/v-%) under stirring at 50 °C for 48 h. Next, 100 mL of distilled water was added to the system, which was centrifuged (5000 rpm for 10 min) to collect the precipitate, and the water-adding and centrifugation process was repeated two more times. The CsNWs suspension was dialyzed against distilled water (molecular weight cut-off 12,000 g/mol) for 72 h at room temperature (~25 °C) until neutral pH. The pH of this aqueous CsNWs supernatant was adjusted to 3 using 1 mol/L HCl, then homogenized by sonication. Finally, the suspension was centrifuged (3000 rpm for 5 min) to remove last remaining precipitate. The CsNWs yield was 74 % as compared with the CtNWs initial mass. CsNWs suspension (1.0 w/v-% or 10 mg/mL) was stored in a fridge (8 °C) prior to its use.

2.4. Fabrication of the nanofiber mats

2.4.1. CA nanofibers

CA homogeneous solution was prepared by dissolving it in 2:1 v/v acetone:DMAc solution (total volume 10 mL) under stirring for 24 h at room temperature (~25 °C). The solution concentration was fixed at 15 w/v-% of CA (i.e., 1.5 g of CA in 10 mL of acetone:DMAc). Next, this solution was electrospun using the same protocol described by Liu et al. (Liu & Hsieh, 2002) with slight modification. The CA solution (10 mL) was put into a 20 mL syringe (Henk Sass Wolf, Germany) equipped with

a metal 21 or 24-gauge needle. Then, the solution was spun under a 14 kV using a DC power supply (0–30 kV, Gamma High Voltage Research Inc., USA) and a flow rate of 1 mL/h controlled by a syringe pump (KD Scientific, model KDS 200, USA). The electrospun nanofibers mats were collected in a vertically positioned grounded aluminum plate (30 × 30 cm) located at 25 cm (horizontal direction) from the tip of the needle. The electrospun mats (labeled as CANFs) were vacuum dried at ambient temperature (~25 °C) with 85 % of yield (~1.3 g).

2.4.2. CA nanofibers filled with CtNWs

The nanofibers filled with CtNWs were fabricated using a similar protocol; however, specific amounts of CtNWs (0.5 or 2.5 w% in relation to CA mass) were added in CA solutions before the electrospun process. These mats were labeled as CANFs-CtNWs0.5 and CANFs-CTNWs2.5, respectively.

2.4.3. CA nanofibers coated by CsNWs

The as-fabricated CANFs were coated with CsNWs via a physical adsorption. Briefly, CANFs samples (5 mg) were immersed in a CsNWs aqueous suspension (20 mL, 1 mg/mL, pH 3) for 3 h at room temperature (~25 °C). Next, the coated nanofibers mats (labeled as CANFs-CsNWs) were recovered and rinsed in distilled water for 5 min. This rinsing process was repeated three times. Finally, the CANFs-CsNWs were vacuum dried at ambient temperature prior to characterization.

2.5. Characterization techniques

The chemical nature of the electrospun nanofibers was examined by Fourier Transform Infrared (FTIR) spectroscopy. The spectra of samples pressed with KBr were obtained in a Nicolet 6700 (Thermo Electron Corporation, USA) spectrophotometer operating in the region from 400 to 4000 cm^{-1}, at a resolution of 4 cm^{-1} and 64 scan acquisitions. Field-Emission Scanning Electron Microscopy (FE-SEM) was used to investigate the morphology of the nanofibers. Herein, dried samples were sputtered coated with gold, then, imaged by FE-SEM (FI/Philips model XL 30-SFEG, USA) operating at a 5 mm working distance and 5-kV accelerating voltage. Fiber diameter distribution was measured using ImageJ® software from 100 randomly fibers in different FE-SEM images of the same sample. The X-ray diffraction (XRD) patterns of the nanofiber samples were obtained in a Sintag powder diffractometer (model XDS 2000, USA) equipped with a Ni-filtered Cu-Kα radiation source operating at an anode voltage of 45 kV and a current of 40 mA. XRD patterns were obtained in a scanning range of 5–50° with a scanning rate of 1°/min. The crystallinity was calculated per Eq. (1):

$$C = \frac{A_C}{A_T}\ x\ 100 \quad (1)$$

where A_C is the total area under the crystalline diffraction peaks and A_T is the total area under the curve $2\theta = 5°$ to 30°. The deconvolution method was used to resolve the individual peaks. The data was smoothed using 10 points in a second-order regression based on the Savitzky-Golay filter, then deconvoluted based on Gaussian or Lorentzian functions in the OriginPro® software (version 8.5, USA). Thermogravimetric analyses (TGA) were performed in a Shimadzu TGA50 Analyzer (Japan) equipment operating in a temperature range of 30–550 °C at a heating rate of 10 °C/min under $N_{2(g)}$ atmosphere (flow of 50 mL/min). Differential Scanning Calorimetry (DSC) thermograms were recorded in a Shimadzu DSC-60 calorimeter (Japan) operating in a temperature range of 30–550 °C at a heating rate of 10 °C/min under N_2 atmosphere (flow of 30 mL/min). Zeta potential measurements were done in a Malvern ZetaSizer (model NanoZS90, USA) equipped with an auto-titrator device (MPT-2). The nanofibers samples (~10 mg) were immersed in an HCl solution (20 mL, pH 2) and sonicated for 6 min. By adding 0.5 (mol/L) NaOH, different pH values (from 2 to 12) were achieved in which the zeta potential was measured.

2.6. Antibacterial activity

The antibacterial activity of nanofiber mats was assessed using *Escherichia coli* (*E. coli*) ATCC 26922 as model microorganism. The number of living cells was determined by the viable counting method (Rauf et al., 2019; Xu et al., 2011). Firstly, 950 μL of nanofibers mats or 300 μL CsNWs suspensions were transferred to Eppendorfs containing 50 μL of *E. coli* (5×10^7 CFU/mL). The volume was adjusted to 1 mL using a physiological saline solution. Then, the samples were incubated at 37 °C for 1 and 24 h. Aliquots were collected from the supernatant and diluted with Tryptic Soy Broth (TSB) to a final concentration of 10^4 CFU/mL. Then, 30 μL were added to Tryptic Soy Agar (TSA) plates and incubated at 37 °C for 24 h, prior CFU counting. A sterile physiological saline solution was used as control. The minimum inhibitory concentration (MIC) for CsNWs was 117 μg/mL and for CANFs the MIC was negligible. All experiments were performed in triplicates.

2.7. Evaluation of cytotoxicity

Vero cells (kidney epithelial cells extracted from an African green monkey) were cultivated in DMEM supplemented with 2 mmol/L of L-glutamine and 10 % of fetal bovine serum (FBS). The cells were quantified and seed to 24 wells plates at 2.5×10^5 cells/mL and incubated at 37 °C and 5 % CO_2. After 12 h, the culture medium was substituted by DMEM free of serum, then polymer fragments (1 cm^2) were added, followed by 72 h of incubation. Cell viability was determined by MTT assay (Mosmann, 1983). Cells cultivated in the absence of membranes were used as control.

2.8. Statistical analysis

The data were analyzed by one-way analysis of variance (ANOVA) followed by Newman-Keuls test. All analyses were performed using the OriginPro® software (version 8.5, USA). Data are expressed as mean ± standard error of the mean. Also, $p < 0.05$ was considered statistically significant.

3. Results and discussion

3.1. Characterization of the nanofibers mats

CA dissolved easily in 2:1 v/v acetone/DMAc mixture, forming a clear solution at 15 w%. Aqueous CtNWs suspension (up to 7.5 w%) at pH 3 appeared homogeneous and slightly translucent, indicating excellent dispersibility without precipitates (Pereira et al., 2014). Mixing aqueous CtNWs suspension with CA solution caused slight opalescence, due to the presence of 5 % water that is a non-solvent for CA. The CtNWs containing solutions remained homogeneous and with no precipitation, indicating the solubility of CA was not significantly affected by the addition of such a small percentage of water. Pure CA solutions could be electrospun smoothly and continuously under the conditions used. Electrospinning of CA/CtNWs mixtures, however, showed considerable gelation at the needle tip in ca. 20 min that was resolved by reducing the needle size from 21 to 24 gauge, or ca. 0.5 mm to 0.3 mm inner diameter.

Electrospun CANFs appears as a white mat with uniform texture and could be easily detached from the aluminum foil collector. SEM images show the CANFs to be straight and uniform along the lengths of fibers and well separated individual fibers with average diameter of 563 ± 222 nm and lengths at least several millimeters (Fig. 1a and b). The addition of CtNWs did not change the gross appearance of the mats as evident of well spatially distributed fibers (Fig. 1c and e); however, the fiber diameters were significantly reduced to 223 ± 76 nm for the CANFs-CtNWs0.5 (Fig. 1c and d) and 240 ± 102 nm for CANFs-CtNWs2.5 (Fig. 1e and f). It is evident that the addition of CtNWs reduced fiber diameters as the extent of diameter reduction exceeds the reduced

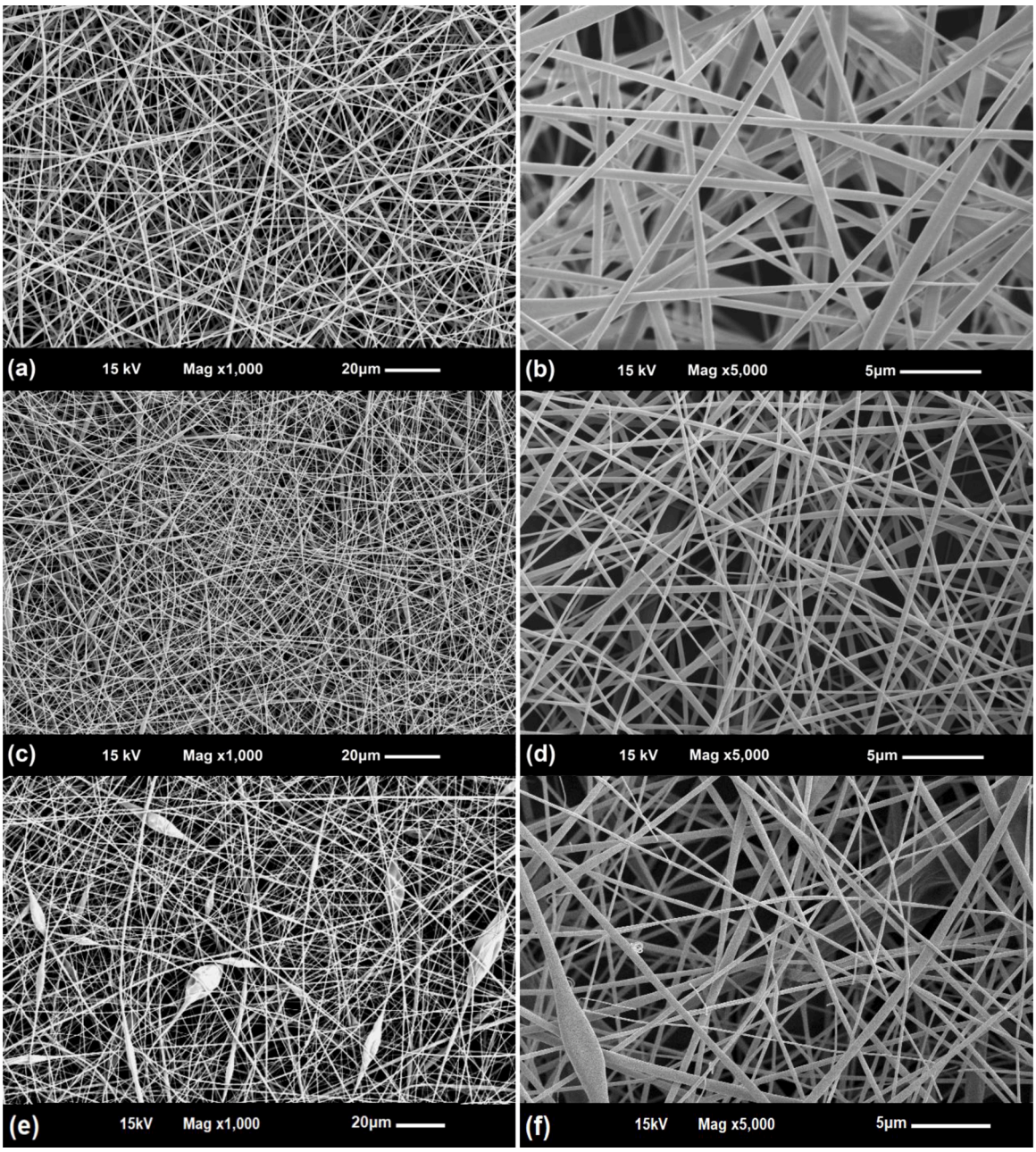

Fig. 1. SEM images of (a,b) CANFs, (c,d) CANFs-CtNWs0.5, and (e,f) CANFs-CtNWs2.5.

spinneret size. This effect resulted from the charged nature of CtNWs, which increased the electrical conductivity of the CtNWs-containing CA solution. Therefore, the polymer jet in the electrospinning process was accelerated and stretched more than the jet in pure CA solution, leading to decreased diameter of final fibers. This effect is consistent with what has been reported (Haider, Haider, & Kang, 2018). Besides, the as-spun mats at the higher 2.5 w% CtNWs showed more varying fiber size as well as some beads, indicative of impaired electrospinning due to the higher amounts of CtNWs.

FTIR spectra of CANFs, CANFs-CtNWs0.5, CANF-CtNWS2.5, and CtNWs to confirm the presence of the CtNWs filler within the nanofibers mats (Fig. 2a). The spectrum of CANFs exhibited a broad band centered at 3475 cm^{-1} (O—H stretching of hydroxyl groups), bands in 2950–2890 cm^{-1} region (C-H stretching of CH_x groups), bands at 1744 cm^{-1} (C=O stretching of carbonyl group), and bands at 1372 cm^{-1} (C-CH_3stretching), 1244 cm^{-1}—(C-O-C anti-symmetric stretching ester group) and 906 cm^{-1} (a combination of —C-O stretching and CH_2 rocking vibrations) (Rieger, Porter, & Schiffman, 2016). Also, the band at 1646 cm^{-1} can be associated with the presence of water molecules (Sudiarti, Wahyuningrum, Bundjali, & Made Arcana, 2017). CtNWs spectrum showed the chitin characteristic absorption bands at 3450 cm^{-1}—(O-H stretching), 3264 cm^{-1} and 3103 cm^{-1} (N-H stretching), 2900–2800 cm^{-1} region (—C-H stretching), 1655 cm^{-1} (amide I), 1560 cm^{-1} (amide II), 1166 cm^{-1}— (C-N stretching), and 1070 cm^{-1} (C-O stretching) (Pereira et al., 2014). With low CtNWs added, the FTIR of CANFs-CtNWs0.5 showed no noticeable change from CANFs, suggesting the filler to be below the limit of detection and without observable interaction with CA, and at this small concentration, it is not perceptible. On the other hand, the CANFs-CtNWs2.5 spectrum exhibited the presence of CtNWs with chitin characteristic bands at 3264 cm^{-1} and 3105 cm^{-1} (N-H stretching, 1560 cm^{-1} (amide II), and 1070 cm^{-1} (C-O stretching). Furthermore, no changes in the position of the bands associated with CA were observed, suggesting weak interaction between the CA matrix and the CtNWs filler.

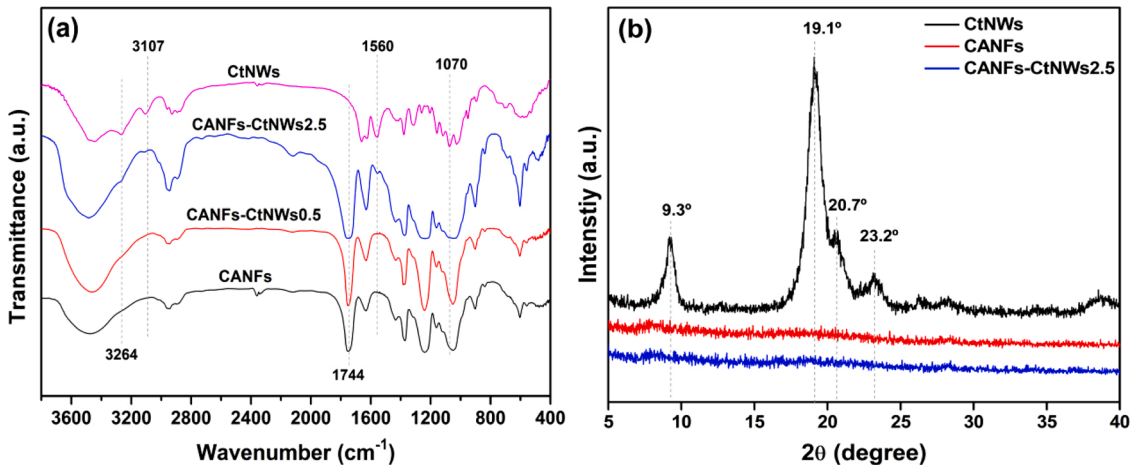

Fig. 2. (a) CANFs, CANFs-CtNWs0.5, CANF-CtNWS2.5, and CtNWs. (b) XRD patterns of CtNWs, CANFs, and CANFs-CtNWS2.5.

The XRD pattern of CtNWs exhibited diffraction peaks at 2θ≈9.3°, 19.1°, 20.7°, 23.2°, and 26.2° (Fig. 2b) corresponding to the (020), (110), (120), (130), and (013) crystallographic planes of chitin (Beibei Ding et al., 2012; Minke & Blackwell, 1978; Pereira et al., 2014). The crystallinity of CtNWs was calculated to be 86 %, which corroborates with our previous study (Pereira et al., 2014). The CANFs pattern did not exhibit any diffraction peak due to the amorphous nature of the nanofibers (Hamano et al., 2016). For the CANF-CtS2.5 mats, CA in the CtNWs-containing nanofibers were also amorphous, similar to CANFs, and the diffraction peaks of CtNWs were not observed, due likely to the extent below the detection level.

Thermal analysis (DSC and TGA/DTG) were used to examine the effect of CtNWs addition on the thermal stability of CANFs. At compositions up to 2.5 w% CtNWs, no significant effect was observed (Fig. 3). DSC curve of CtNWs showed one exothermic broad peak in the temperature range of 250–450 °C (Fig. 3a) associated with its thermal degradation. The DSC curve of CANFs showed four thermal transitions. The first transition occurred in the temperature range of 50–100 °C due

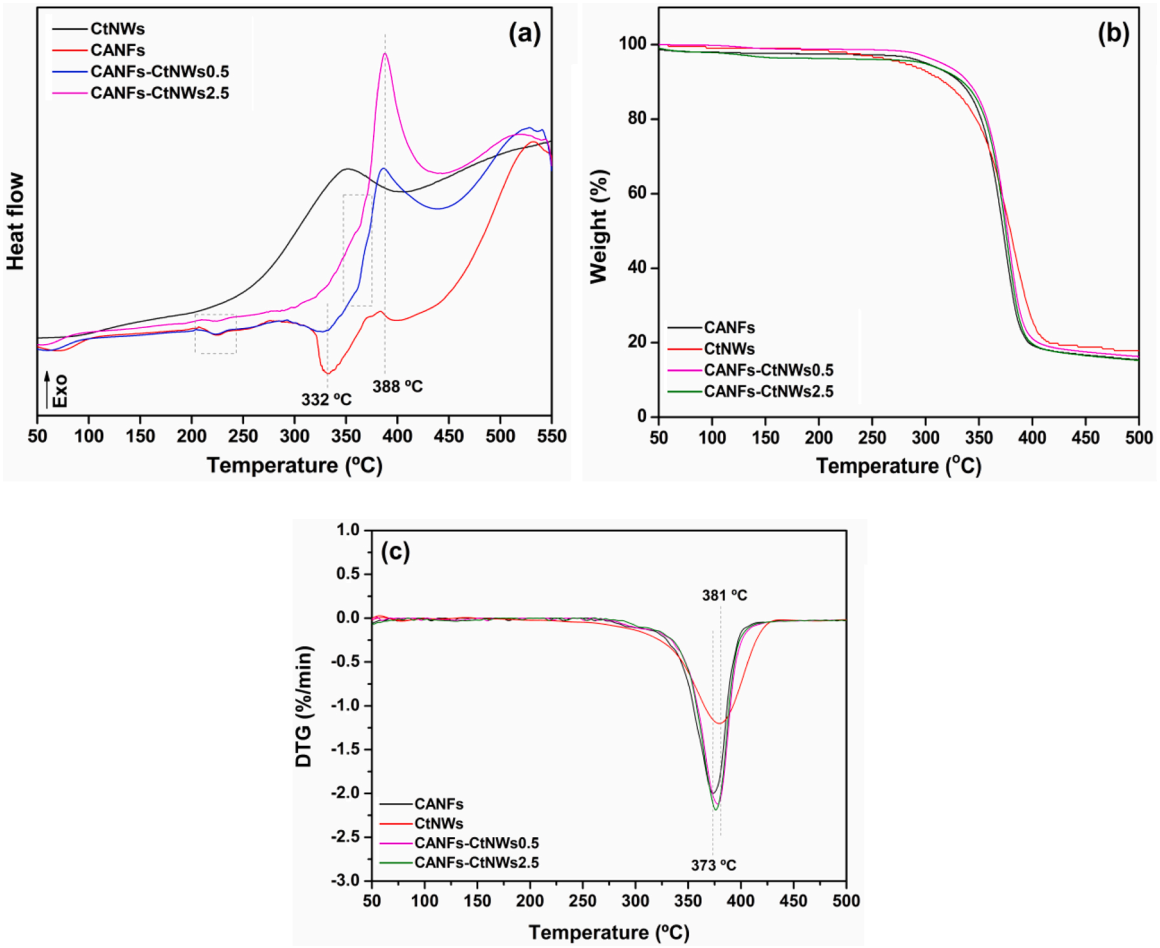

Fig. 3. (a) DSC, (b) TGA, and (c) DTG curves obtained for CANFs, CtNWs, CANFs-CtNWS0.5, and CANFs-CtNWS2.5.

to the evaporation of adsorbed water. Besides, a minimal baseline change (endothermic shoulder) around 225 °C is attributed to Tg of CA (Kendouli et al., 2014), followed by two endothermic peaks centered at 332 °C and 400 °C attributed to degradation stages of the polysaccharide. The DSC curve of CANFs filled with CtNWs (0.5 or 2.5 w%) showed reduced moisture endothermic peaks and barely distinguishable endothermic transitions. For the mat containing the lowest amount of CtNWs, the endothermic peak around 225 °C was slightly reduced as compared to CANFs. In comparison, the exothermic peak associated with the degradation of CtNWs was sharpened and shifted to a high-temperature range (maximum at 388 °C). Moreover, the first endothermic peak ascribed to the decomposition of CA (at 332 °C) was reduced. For the CANFs-CtNWS2.5 sample, this endothermic peak was not observed, which may indicate an interaction between CA and CtNWs by hydrogen bonding or hydrophobic interactions, considering the chemical nature of these two compounds. Again, an intense endothermic peak is still observed at 388 °C due to the thermal degradation of CtNWs filled in CANFs-CtNWS2.5.

TGA/DTG curves of pure CtNWs, CANFs, CANFs-CtNWS0.5, and CANFs-CtNWS2.5 shown in Fig. 3b and c. For CANFs, a one stage weight-loss of ~85 % was noticed occurring from 200 to 450 °C with a maximum temperature at 373 °C. The TGA curve of CtNWs also exhibited one weight loss state with a maximum temperature at 381 °C (weight loss ~85 %). Although it is expected some interaction between CtNWs and CANFs, as noticed from the TGA/DTG curves, the addition of different amounts of CtNWs did not change the thermal stability of CANFs mats, independent of loading level. Similar to CANFs mat, the TGA curves for CANFs-CtNWS0.5 and CANFs-CtNWS2.5 exhibited major weight loss at maximum temperature around 373 °C.

From these preliminary analyses, it was concluded that the addition of CtNWs on the bulk phase of CANFs exerted only a slight effect on the properties examined . Focusing on the modification of surface properties of the CANFs, an alternative approach to took advantage of the fact that CANFs are negatively charged at surface was investigated by depositing CsNWs, a deacetylated CtNW-derivative, that can be positively charged by protonating surface amino groups under acidic conditions (Pereira et al., 2014).

The surface charge properties of CANFs as is and with coated nanowhiskers were measured to derive their zeta potential (ζ) values under a full range of pH. CANFs exhibited ζ around −40 mV from pH 4 to pH 10 as expected (Fig. 4). With coated CsNWs, the CANFs-CsNWs showed complete reversal to ζ around +8 mV from pH 2 to pH 10, confirming the successful adsorption of cationic CsNWs on anionic CANFs surfaces by electrostatic interactions. The ζ for aqueous CsNWs suspension was around +40 mV (at pH < 6), which is an indicative of their high stability under neutral and acidic conditions (Pereira et al., 2014). While the surface adsorbed CsNWs more than neutralized the negative charged CANFs, the lower positive zeta potential of CANFs-CsNWs than CsNWs suggests CANF surfaces to be partially covered with CsNWs under the condition studied. -However, complete reversal of ζ was not observed for electrospun CA coated with chitin nanocrystals (Goetz et al., 2016). The ζ of CtNWs and CANFs-CtNWs2.5 were also measured for comparison. While lower than CsNWs, the predominant positively charged CtNWs under acidic conditions (pH < 6) suggest partial hydrolysis the chitin moieties on their surfaces. However, when CtNWs were internally doped, the resulting CANFs-CtNWs2.5 had similarly negative charges as CANFs, indicating CtNWs to be imbedded in the bulk of the fiber thus ineffective in altering surface charge characteristics. Intriguingly, upon heating at 180 °C for 4 h, CANFs-CtNWs2.5(180°) also exhibited positive zeta potential similar to CANFs-CsNWs. This confirms that the initially embedded inside the nanofibers surfaced upon heating to be responsible for the positive charge over a large pH range (CANFs-CtNWs2.5(180°)).

These zeta potential data are also useful to determine the isoelectric point (IP) on pH values where there is no net surface charge. The IPs derived were pHs at 2.7, 7.3 and 8.3, 9.9, 10.3, and 10.5 for CANFs, CtNWs, CsNWs, CANFs-CsNWs, CANFS-CtNWs2.5, and CANFS-CtNWs2.5(180°), respectively. These surface charge characteristics showed the surface adsorption of CsNWs approach to be indeed most effective to modify the surface properties of the fibers. It is essential to highlight that surface properties could be changed by merely immersing CANFs in diluted CsNW suspensions. These drastic alterations of surface charge nature of cellulose fibrous mats by surface adsorption or simple dip coating with either chitin or chitosan nanowhiskers are successfully demonstrated and reported for the first time.

The SEM of CANFs-CsNWs mat showed similar smooth morphology and texture as CANFs and without any change in overall fiber distribution nor porosity, Fig. 5. The average diameter of the nanofibers was 430 ± 194 nm, statistically the same as that of CANFs.

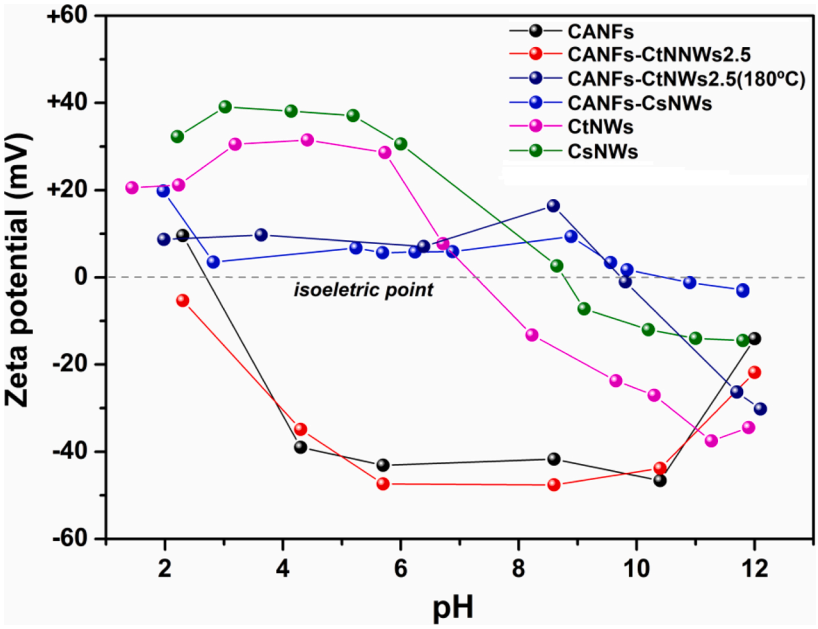

Fig. 4. Zeta potential (ζ) data over pH for whiskers and nanofibrous mats.

3.2. Antibacterial activity and cytotoxicity studies

The antibacterial assays of CsNWs, CANFs, and CANFs-CsNWs against *E. coli*, common and naturally occurring bacillar bacteria in the human intestine that cause serious infections when present in food, water, and bloodstream (Katouli, 2010), are displayed in Fig. 6. As shown in agar plates (Fig. 6), both CsNWs and CtNWs reduced *E. coli* cell viability slightly while CANFs-CsNWs showed greater reduction in 1 h than CANFs that were not biologically active. These antibacterial activities were more pronounced observed for CsNWs and CtNWs and, for CANFs-CsNWs mats after 24 h. Although CtNWs and CsNWs presented antibacterial activity, it was lower than that observed for CANFs-CsNWs. That anchoring at the CANFs surfaces provided CsNWs stability to continuous interact with E. coli cells for longer times and optimize the bacteriostatic effect is a significant finding. The saline solution used in the culture medium as well as the liberation of cell components may shield the charged groups of CsNWs to promote aggregation, decreasing antibacterial effect and/or reducing suspension of free CsNWs as compared to those bound to CANF membrane.

The colony-forming units (CFU) of samples as a function of time are presented in Fig. 7a. CsNWs inhibited around 34 % of *E. coli* for 1 h of contact. The inhibitory effect increased to 85 % for the longest contact time (24 h). The minimum inhibitory concentration (MIC) was calculated to be 117 μg/mL of CsNWs. The antibacterial activity of CANFs was minimum even after 24 h of contact (~35 % of reduction); however, it was calculated a decrease of 99 % of CFU when it was coated with CsNWs.

The antibacterial activity efficiency of chitin/chitosan depends on several factors: i) microorganism type; ii) charge density, molar mass, and concentration; iii) physical state such as a solid or in solution; iv) environmental condition such as pH, ionic strength, temperature and contact time (Kong, Chen, Xing, & Park, 2010; Martins et al., 2014). Gram-negative bacteria, like *E. coli*, have an external lipopolysaccharides (LPS) cell layer, which consists of lipidic compounds, and an inner LPS layer, that bear anionic carboxylate and phosphate groups to stabilize the membrane by interacting with divalent ions. The antimicrobial effect of chitin and chitosan is thus attributed to the electrostatic attraction between their positively charged–NH_3^+ with those negatively charged (R-COO-, R-OPO$(O_2)^{2-}$) bacterial external cellular membrane to destabilize and damage leading to cell death (Helander, Nurmiaho-Lassila, Ahvenainen, Rhoades, & Roller, 2001). At above IP or pH > pKa of amino groups, in which there are no positive charges on chitin/chitosan, the action mode of such molecules on bacteria is different. The amino groups act as chelating agents binding to the divalent cations of the cellular membrane promoting the antibacterial activity (Sahariah & Másson, 2017). The fact that both CtNWs and CsNWs presented significant inhibition effect against *E. coli* may also relate to their nano-scale dimensions and high specific surface and a large number of surface amino groups available, increasing the interaction with the bacterial cell membrane. Goetz et al. also demonstrated the antibacterial activity induced by chitin nanocrystals on coated CA electrospun mats (Goetz et al., 2016).

The antibacterial activity of CANFs-CsNWs against *E. coli* is similar to that of other electrospun CA or cellulose that contained conventional metal nanoparticles (Ag, Ni, Co, Cu) and metal oxides (ZnO, CuO) as antimicrobial agents. Most importantly, CANFs-CsNWs is advantageous over the use of toxic and expensive reducing agents, advanced techniques (laser ablation) or complicated steps in their preparation (Ahmed, Menazea, & Abdelghany, 2020; Demirdogen et al., 2020; Jatoi, Kim, & Ni, 2019; Wu, Qiu, Wang, Zhang, & Qin, 2019). This fact highlights the potential of the CANFs-CsNWs for more sustainable and biocompatible applications.

Another crucial aspect of materials in the biomedical field is the cytotoxic effects on healthy cells. Herein, the cytotoxicity of CANFs and CANFs-CsNWs towards Vero cells were assessed by cell viability after 72 h of incubation (Fig. 7b). For all samples studied, the cell viability was higher than the control (absence of fibrous mats), indicating the samples not to be toxic to the healthy cells. Also, the higher cell viability when incubated with CANFs and CANFs-CsNWs than that with the control indicates that both mats increase cell density. In summary, the absence of cytotoxicity in combination with the remarkable antibacterial properties ranks CANFs-CsNWs as a promising material for medical applications.

4. Conclusion

This study has validated the hypothesis that chitin (CtNWs) and chitosan nanowhiskers (CsNWs) change the surface properties of electrospun cellulose acetate nanofibers (CANFs) to induce biological activity. Physical adsorption of CsNWs on the as-prepared CANFs was proven to be most effective and facile, switching the negatively charged CANFs ($\zeta = -40$ mV) to positively charged CANFs-CsNWs ($\zeta = +8$ mV). While CANFs-CtNWs prepared by doping CtNWs in CA did not produce any effect, heat treatment has shown to mobilize CtNWs to fiber surfaces to exert similar surface charge effect. Although zeta potential of CANFs-CsNWs was not as highly positive as pure CsNWs, suggesting the CANFs surfaces not to be fully covered by CsNWs, the coverage was sufficient to promote significant changes in biological features, i.e., effective in reducing 99 % of CFU of Gram-negative bacterium, *E. coli,* in 24 h and atoxic to Vero cells. SEM images showed the CsNWs coverage did not change the smooth and homogeneous morphology of fibers.

The concept of modifying materials surfaces by electrostatic attraction of cationically charged CsNWs to anionically charged cellulose fibers has been proven and validated. This facile approach has been demonstrated to be effective in inducing biological properties to present enormous potential to be applied to a wide scope of fields including tissue engineering, wound dressing, filtration systems, diapers, and hygienic products, among others. Moreover, the developed material is

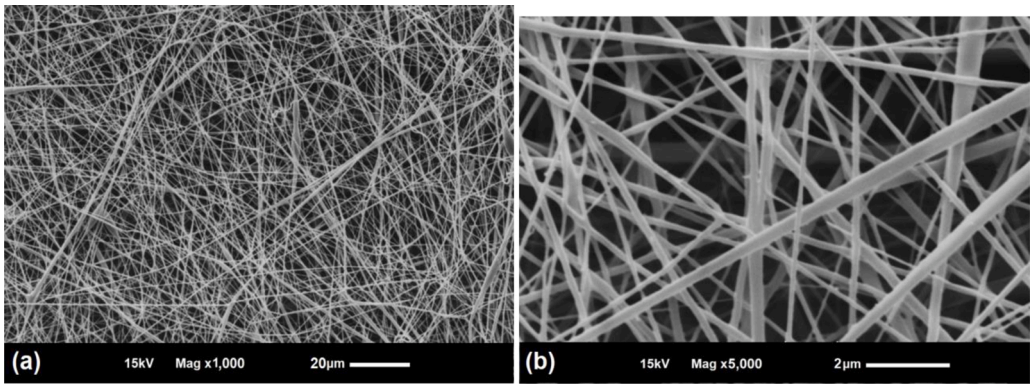

Fig. 5. SEM images of CANFs-CsNWs at different magnifications. (a) Mag ×1000 and (b) Mag ×5000.

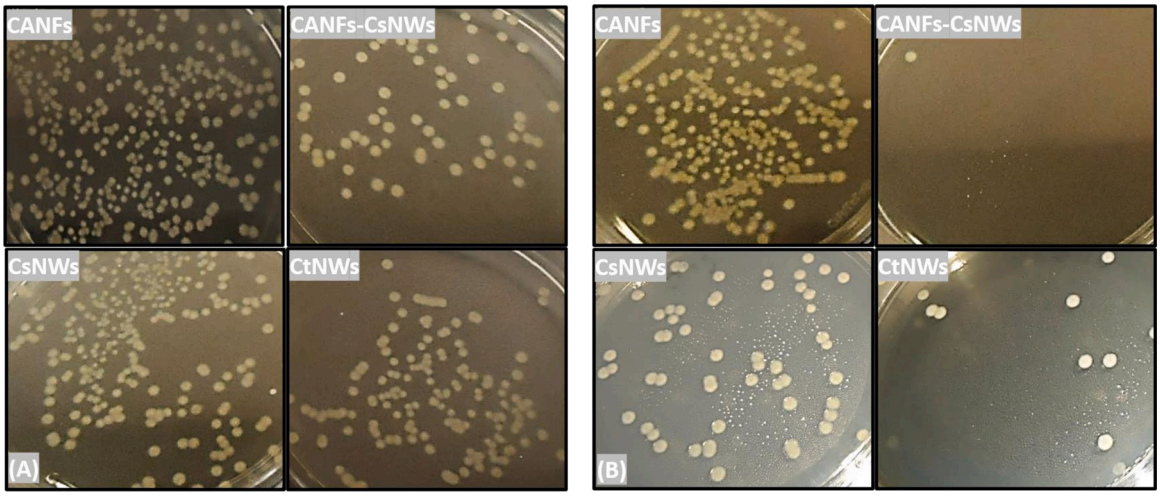

Fig. 6. Antibacterial activities of CsNWs, CANFs, and CANFs-CsNWs against *E. coli* tested in Agar plates for (A) 1 h and (B) 24 h of contact time.

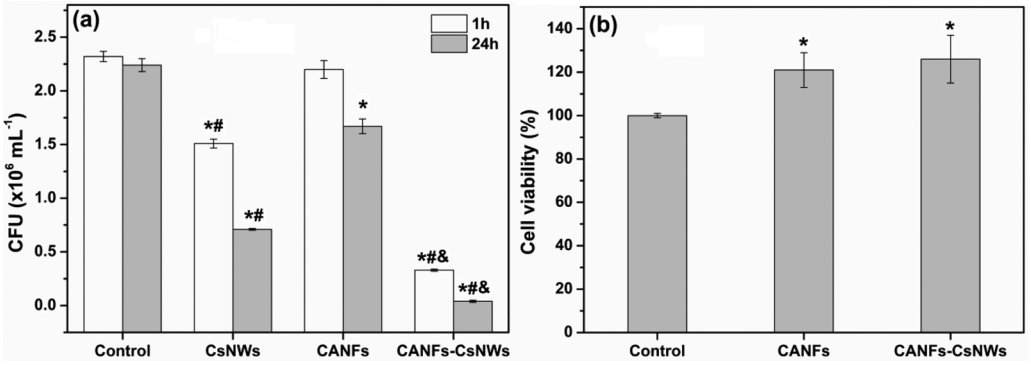

Fig. 7. (a) Effect of CsNWs, CANFs, CANFs-CsNWs against *E. coli* for different time intervals. (b) Cytotoxic of CANFs and CANFs-CsNWs against *Vero* cells line after 72 h of incubation. Data represent the mean ± S.E.M. (one-way ANOVA). $^{*}p < 0.05$ compared with the control group, $^{\#}p < 0.05$ compared CANFs group, $^{\&}p < 0.05$ compared with CsNWs group.

based on the two most abundant polysaccharides, i.e., cellulose, and chitin, to be biocompatible, biodegradable, and renewable. Further studies on the effect of different degrees of CsNWs deposition on charge nature and antibacterial activity as well as on mechanical properties of electrospun mats will enable more potential applications of CANFs-CsNWs.

CRediT authorship contribution statement

Antonio G.B. Pereira: Formal analysis, Methodology, Writing - original draft. **André R. Fajardo:** Methodology, Writing - original draft. **Adriana P. Gerola:** Formal analysis. **Jean H.S. Rodrigues:** Formal analysis. **Celso V. Nakamura:** Supervision. **Edvani C. Muniz:** Supervision. **You-Lo Hsieh:** Conceptualization, Supervision.

Declaration of Competing Interest

The authors report no declarations of interest.

Acknowledgments

A.G.B. Pereira is grateful to Dr. F. Jiang for the assistance on SEM and XRD and to CAPES for the fellowship (Process BEX 2394/11-1) as a visiting scholar at University of California, Davis, USA. A.R.F is thankful to CNPq for his PQ fellowship (Process 304711/2018-7).

References

Ahmed, M. K., Menazea, A. A., & Abdelghany, A. M. (2020). Blend biopolymeric nanofibrous scaffolds of cellulose acetate/ε-polycaprolactone containing metallic nanoparticles prepared by laser ablation for wound disinfection applications. *International Journal of Biological Macromolecules*. https://doi.org/10.1016/J.IJBIOMAC.2020.03.257.

Anitha, S., Brabu, B., Thiruvadigal, D. J., Gopalakrishnan, C., & Natarajan, T. S. (2012). Optical, bactericidal and water repellent properties of electrospun nano-composite membranes of cellulose acetate and ZnO. *Carbohydrate Polymers, 87*(2), 1065–1072. https://doi.org/10.1016/j.carbpol.2011.08.030.

Antunes, J. C., Pereira, C. L., Molinos, M., Ferreira-da-Silva, F., Dessì, M., Gloria, A., et al. (2011). Layer-by-layer self-assembly of chitosan and poly(γ-glutamic acid) into polyelectrolyte complexes. *Biomacromolecules, 12*(12), 4183–4195. https://doi.org/10.1021/bm2008235.

Bai, L., Kämäräinen, T., Xiang, W., Majoinen, J., Seitsonen, J., Grande, R., et al. (2020). Chirality from cryo-electron tomograms of nanocrystals obtained by lateral disassembly and surface etching of never-dried chitin. *ACS Nano, 14*(6), 6921–6930. https://doi.org/10.1021/acsnano.0c01327.

Beier, S. P., Guerra, M., Garde, A., & Jonsson, G. (2006). Dynamic microfiltration with a vibrating hollow fiber membrane module: Filtration of yeast suspensions. *Journal of Membrane Science, 281*(1–2), 281–287. https://doi.org/10.1016/J.MEMSCI.2006.03.051.

Berger, J., Reist, M., Mayer, J., Felt, O., & Gurny, R. (2004). Structure and interactions in chitosan hydrogels formed by complexation or aggregation for biomedical applications. *European Journal of Pharmaceutics and Biopharmaceutics, 57*(1), 35–52. https://doi.org/10.1016/S0939-6411(03)00160-7.

Chen, H., & Hsieh, Y.-L. (2005). Enzyme immobilization on ultrafine cellulose fibers via poly(acrylic acid) electrolyte grafts. *Biotechnology and Bioengineering, 90*(4), 405–413. https://doi.org/10.1002/bit.20324.

Dash, M., Chiellini, F., Ottenbrite, R. M., & Chiellini, E. (2011). Chitosan—A versatile semi-synthetic polymer in biomedical applications. *Progress in Polymer Science, 36*(8), 981–1014. https://doi.org/10.1016/J.PROGPOLYMSCI.2011.02.001.

Demirdogen, R. E., Kilic, D., Emen, F. M., Aşkar, Ş., Karaçolak, A.İ., Yesilkaynak, T., et al. (2020). Novel antibacterial cellulose acetate fibers modified with 2-fluoropyridine

complexes. *Journal of Molecular Structure, 1204*, Article 127537. https://doi.org/10.1016/J.MOLSTRUC.2019.127537.
Ding, B., Cai, J., Huang, J., Zhang, L., Chen, Y., Shi, X., et al. (2012). Facile preparation of robust and biocompatible chitin aerogels. *Journal of Materials Chemistry, 22*(12), 5801–5809. https://doi.org/10.1039/C2JM16032C.
Ding, B., Du, J., & Hsieh, Y.-L. (2011). Tubular multi-bilayer polysaccharide biofilms on ultra-thin cellulose fibers. *Journal of Applied Polymer Science, 121*(5), 2526–2534. https://doi.org/10.1002/app.33955.
Doshi, J., & Reneker, D. H. (1995). Electrospinning process and applications of electrospun fibers. *Journal of Electrostatics, 35*(2), 151–160. https://doi.org/10.1016/0304-3886(95)00041-8.
Du, J., & Hsieh, Y.-L. (2009). Cellulose/chitosan hybrid nanofibers from electrospinning of their ester derivatives. *Cellulose, 16*(2), 247–260. https://doi.org/10.1007/s10570-008-9266-9.
Elashnikov, R., Rimpelová, S., Děkanovský, L., Švorčík, V., & Lyutakov, O. (2019). Polypyrrole-coated cellulose nanofibers: Influence of orientation, coverage and electrical stimulation on SH-SY5Y behavior. *Journal of Materials Chemistry B, 7*(42), 6500–6507. https://doi.org/10.1039/C9TB01300H.
Goetz, L. A., Jalvo, B., Rosal, R., & Mathew, A. P. (2016). Superhydrophilic anti-fouling electrospun cellulose acetate membranes coated with chitin nanocrystals for water filtration. *Journal of Membrane Science, 510*, 238–248. https://doi.org/10.1016/j.memsci.2016.02.069.
Haider, S., & Park, S.-Y. (2009). Preparation of the electrospun chitosan nanofibers and their applications to the adsorption of Cu(II) and Pb(II) ions from an aqueous solution. *Journal of Membrane Science, 328*(1–2), 90–96. https://doi.org/10.1016/J.MEMSCI.2008.11.046.
Haider, A., Haider, S., & Kang, I.-K. (2018). A comprehensive review summarizing the effect of electrospinning parameters and potential applications of nanofibers in biomedical and biotechnology. *Arabian Journal of Chemistry, 11*(8), 1165–1188. https://doi.org/10.1016/j.arabjc.2015.11.015.
Hamano, F., Seki, H., Ke, M., Gopiraman, M., Lim, C. T., & Kim, I. S. (2016). Cellulose acetate nanofiber mat with honeycomb-like surface structure. *Materials Letters, 169*, 33–36. https://doi.org/10.1016/J.MATLET.2015.11.069.
Helander, I., Nurmiaho-Lassila, E.-L., Ahvenainen, R., Rhoades, J., & Roller, S. (2001). Chitosan disrupts the barrier properties of the outer membrane of Gram-negative bacteria. *International Journal of Food Microbiology, 71*(2–3), 235–244. https://doi.org/10.1016/S0168-1605(01)00609-2.
Jatoi, A. W., Kim, I. S., & Ni, Q. Q. (2019). A comparative study on synthesis of AgNPs on cellulose nanofibers by thermal treatment and DMF for antibacterial activities. *Materials Science and Engineering: C, 98*, 1179–1195. https://doi.org/10.1016/J.MSEC.2019.01.017.
Jia, Y., Yu, H., Zhang, Y., Dong, F., & Li, Z. (2016). Cellulose acetate nanofibers coated layer-by-layer with polyethylenimine and graphene oxide on a quartz crystal microbalance for use as a highly sensitive ammonia sensor. *Colloids and Surfaces B: Biointerfaces, 148*, 263–269. https://doi.org/10.1016/J.COLSURFB.2016.09.007.
Katouli, M. (2010). Population structure of gut Escherichia coli and its role in development of extra-intestinal infections. *Iranian Journal of Microbiology, 2*(2), 59–72. https://pubmed.ncbi.nlm.nih.gov/22347551.
Kendouli, S., khalfallah, O., Sobti, N., Bensouissi, A., Avci, A., Eskizeybek, V., et al. (2014). Modification of cellulose acetate nanofibers with PVP/Ag addition. *Materials Science in Semiconductor Processing, 28*, 13–19. https://doi.org/10.1016/J.MSSP.2014.03.010.
Kong, M., Chen, X. G., Xing, K., & Park, H. J. (2010). Antimicrobial properties of chitosan and mode of action: A state of the art review. *International Journal of Food Microbiology, 144*(1), 51–63. https://doi.org/10.1016/J.IJFOODMICRO.2010.09.012.
Liu, H., & Hsieh, Y.-L. (2002). Ultrafine fibrous cellulose membranes from electrospinning of cellulose acetate. *Journal of Polymer Science Part B: Polymer Physics, 40*(18), 2119–2129. https://doi.org/10.1002/polb.10261.
Lu, P., & Hsieh, Y.-L. (2009). Lipase bound cellulose nanofibrous membrane via Cibacron Blue F3GA affinity ligand. *Journal of Membrane Science, 330*(1), 288–296. https://doi.org/10.1016/j.memsci.2008.12.064.
Lu, P., & Hsieh, Y.-L. (2010). Multiwalled carbon nanotube (MWCNT) reinforced cellulose fibers by electrospinning. *ACS Applied Materials & Interfaces, 2*(8), 2413–2420. https://doi.org/10.1021/am1004128.
Ma, G., Liu, Y., Peng, C., Fang, D., He, B., & Nie, J. (2011). Paclitaxel loaded electrospun porous nanofibers as mat potential application for chemotherapy against prostate cancer. *Carbohydrate Polymers, 86*(2), 505–512. https://doi.org/10.1016/J.CARBPOL.2011.04.082.
Martins, A. F., Facchi, S. P., Follmann, H. D. M., Pereira, A. G. B., Rubira, A. F., & Muniz, E. C. (2014). Antimicrobial activity of chitosan derivatives containing N-quaternized moieties in its backbone: A review. *International Journal of Molecular Sciences, 15*(11). https://doi.org/10.3390/ijms151120800.
Minke, R., & Blackwell, J. (1978). The structure of α-chitin. *Journal of Molecular Biology, 120*(2), 167–181. https://doi.org/10.1016/0022-2836(78)90063-3.
Mosmann, T. (1983). Rapid colorimetric assay for cellular growth and survival: Application to proliferation and cytotoxicity assays. *Journal of Immunological Methods, 65*(1–2), 55–63. https://doi.org/10.1016/0022-1759(83)90303-4.
Orlova, Y., Magome, N., Liu, L., Chen, Y., & Agladze, K. (2011). Electrospun nanofibers as a tool for architecture control in engineered cardiac tissue. *Biomaterials, 32*(24), 5615–5624. https://doi.org/10.1016/j.biomaterials.2011.04.042.
Pereira, A. G. B., Muniz, E. C., & Hsieh, Y.-L. (2014). Chitosan-sheath and chitin-core nanowhiskers. *Carbohydrate Polymers, 107*, 158–166. https://doi.org/10.1016/J.CARBPOL.2014.02.046.
Pereira, A. G. B., Muniz, E. C., & Hsieh, Y.-L. (2015). 1H NMR and 1H–13C HSQC surface characterization of chitosan–chitin sheath-core nanowhiskers. *Carbohydrate Polymers, 123*, 46–52. https://doi.org/10.1016/J.CARBPOL.2015.01.017.
Quiñones, J. P., Peniche, H., & Peniche, C. (2018). Chitosan based self-assembled nanoparticles in drug delivery. *Polymers, 10*(3), 235. https://doi.org/10.3390/polym10030235.
Rauf, A., Ye, J., Zhang, S., Qi, Y., Wang, G., Che, Y., et al. (2019). Copper(ii)-based coordination polymer nanofibers as a highly effective antibacterial material with a synergistic mechanism. *Dalton Transactions, 48*(48), 17810–17817. https://doi.org/10.1039/C9DT03649K.
Rieger, K., Porter, M., & Schiffman, J. (2016). Polyelectrolyte-functionalized nanofiber mats control the collection and inactivation of Escherichia coli. *Materials, 9*(4), 297. https://doi.org/10.3390/ma9040297.
Ritcharoen, W., Supaphol, P., & Pavasant, P. (2008). Development of polyelectrolyte multilayer-coated electrospun cellulose acetate fiber mat as composite membranes. *European Polymer Journal, 44*(12), 3963–3968. https://doi.org/10.1016/J.EURPOLYMJ.2008.09.023.
Sahariah, P., & Másson, M. (2017). Antimicrobial chitosan and chitosan derivatives: A review of the structure-activity relationship. *Biomacromolecules, 18*(11), 3846–3868. https://doi.org/10.1021/acs.biomac.7b01058.
Sudiarti, T., Wahyuningrum, D., Bundjali, B., & Made Arcana, I. (2017). Mechanical strength and ionic conductivity of polymer electrolyte membranes prepared from cellulose acetate-lithium perchlorate. *IOP Conference Series: Materials Science and Engineering, 223*, Article 012052. https://doi.org/10.1088/1757-899X/223/1/012052.
Tu, H., Wu, G., Yi, Y., Huang, M., Liu, R., Shi, X., et al. (2019). Layer-by-layer immobilization of amphoteric carboxymethyl chitosan onto biocompatible silk fibroin nanofibrous mats. *Carbohydrate Polymers, 210*, 9–16. https://doi.org/10.1016/J.CARBPOL.2019.01.047.
Wang, Y., & Hsieh, Y.-L. (2004). Enzyme immobilization to ultra-fine cellulose fibers via amphiphilic polyethylene glycol spacers. *Journal of Polymer Science Part A: Polymer Chemistry, 42*(17), 4289–4299. https://doi.org/10.1002/pola.20271.
Wu, J., Qiu, Q., Wang, Y., Zhang, H., & Qin, X. (2019). Asymmetric water affinity on antibacterial electrospun sub-micro cellulose acetate Janus membrane. *Materials Letters, 256*, Article 126607. https://doi.org/10.1016/J.MATLET.2019.126607.
Xu, T., Xin, M., Li, M., Huang, H., Zhou, S., & Liu, J. (2011). Synthesis, characterization, and antibacterial activity of N,O-quaternary ammonium chitosan. *Carbohydrate Research, 346*(15), 2445–2450. https://doi.org/10.1016/j.carres.2011.08.002.
Xue, J., Wu, T., Dai, Y., & Xia, Y. (2019). Electrospinning and electrospun nanofibers: Methods, materials, and applications. *Chemical Reviews, 119*(8), 5298–5415. https://doi.org/10.1021/acs.chemrev.8b00593.
Yousef, A., Barakat, N. A. M., Khalil, K. A., Unnithan, A. R., Panthi, G., Pant, B., et al. (2012). Photocatalytic release of hydrogen from ammonia borane-complex using Ni (0)-doped TiO_2/C electrospun nanofibers. *Colloids and Surfaces A: Physicochemical and Engineering Aspects, 410*, 59–65. https://doi.org/10.1016/J.COLSURFA.2012.06.017.
Zhang, L., & Hsieh, Y.-L. (2008). Ultra-fine cellulose acetate/poly(ethylene oxide) bicomponent fibers. *Carbohydrate Polymers, 71*(2), 196–207. https://doi.org/10.1016/j.carbpol.2007.05.031.
Zhang, L., Hsieh, Y.-L., Zhang, L., & Hsieh, Y.-L. (2008). Ultrafine cellulose acetate fibers with nanoscale structural features. *Journal of Nanoscience and Nanotechnology, 8*(9), 4461–4469. https://www.ingentaconnect.com/content/asp/jnn/2008/00000008/00000009/art00023.
Zhang, Y., Venugopal, J. R., El-Turki, A., Ramakrishna, S., Su, B., & Lim, C. T. (2008). Electrospun biomimetic nanocomposite nanofibers of hydroxyapatite/chitosan for bone tissue engineering. *Biomaterials, 29*(32), 4314–4322. https://doi.org/10.1016/j.biomaterials.2008.07.038.
Zhong, Z., Qin, J., & Ma, J. (2015). Cellulose acetate/hydroxyapatite/chitosan coatings for improved corrosion resistance and bioactivity. *Materials Science and Engineering: C, 49*, 251–255. https://doi.org/10.1016/J.MSEC.2015.01.020.